MINBU Distribution of Two Dimensional Quantum Gravity: Simulation Result and Semiclassical Analysis *

S. ICHINOSE †

Department of Physics, Universuty of Shizuoka, Yada 52-1, Shizuoka 422, Japan N. TSUDA [‡]and T. YUKAWA [§] National Laboratory for High Energy Physics(KEK), Tsukuba,Ibaraki 305, Japan

May, 1995

Abstract

We analyse MINBU distribution of 2 dimensional quantum gravity. New data of \mathbb{R}^2 -gravity by the Monte Carlo simulation and its theoretical analysis by the semiclassical approach are presented. The cross-over phenomenon takes place at some size of the baby universe where the randomness competes with the smoothing force of R^2 -term. The dependence on the central charge c_m and on the R^2 -coupling are explained for the ordinary 2d quantum gravity and for R^2 -gravity. The R^2 -Liouville solution plays the central role in the semiclassical analysis. A total derivative term (surface term) and the infrared regularization play important roles . The surface topology is that of a sphere

1 Introduction

The quantum effects of the 2 dimensional (2d) gravitational theories are recently measured numerically in the computer simulation with high statistics. In particular the data for the entropy exponent (string susceptibility) in 2d quantum gravity(QG) is the same as the known exact result within a relative precision of $O(10^{-3})$. It is due to the development of the simulation technique in the dynamical triangulation[1, 2, 3] and the findings of new observables in QG such as MINBU distribution [4, 5, 6].

The data analysis is done by a rather orthodox approach, i.e., the semiclassical approximation. It has recently been applied to $2d R^2$ -gravity and the simulation

^{*}SU-95-05

[†]E-mail address: ichinose@u-shizuoka-ken.ac.jp

[‡]E-mail address: ntsuda@theory.kek.jp [§]E-mail address: yukawa@theory.kek.jp

data of $\langle \int d^2x \sqrt{g}R^2 \rangle$ and its cross-over phenomenon are successfully explained[7]. We list the merits of this approach.

- 1. The semiclassical treatment is, at present, the unique field-theoretical approach which can analyse the mysterious region $(25 \ge) c_m \ge 1$. The conformal field theory gives a meaningful result only for some limitted regions of c_m . The Matrix model is in the similar situation.
- 2. Comparison with the ordinary quantization is transparent because the ordinary renormalizable field theories ,such as QED and QCD, are quantized essentially in the semiclassical way. In particular, the renormalization properties of (2d) QG are expected to be clarified in the semiclassical approch[8].
- 3. This approach can be used for the higher-dimensional QG such as 3d and 4d QG.

The approach is perturbative, therefore choosing the most appropriate vacuum under the global constraints (such as the area constraint and the topology constraint) is crucial in the proper evaluation. We explain it in Sect.3.

We add R^2 -term to the ordinary 2d gravity for the following reasons. (We call the ordinary 2d gravity $Liouville\ gravity$ in contrast with R^2 -gravity for the added one.)

- 1. For the positive coupling, the term plays the role of suppressing the high curvature and making the surface smooth. For the negative one, the high curvature is energetically favoured and making the surface rough. Therefore we can expect a richer phase structure of the surface configuration.
- 2. The term is higher-derivative (∂^4) , therefore it regularizes the ultra-violet behaviour so good[9]. In fact the theory is renormalizable[8].
- 3. The Einstein term (R-term) is topological in 2 dimension. It does not have a local mode. The simplest interaction which is purely geometrical and has local modes is R^2 -term.
- 4. In the lattice gravity, R^2 -term is considered as one of natural irrelevent terms in the continuous limit[10].

The $<\int d^2x\sqrt{g}R^2>$ simulation data for R^2 -gravity was presented by [11] and the cross-over phenomenon was clearly found. We present here MINBU distribution data.

2 Lattice Simulation of 2D Quantum R²-Gravity and MINBU Distribution

The distribution of baby universe (BU) is one of important observables in the lattice gravity [4, 5, 6]. It was originally introduced to measure the entropy exponent (string

susceptibility) efficiently. Fig.1 shows the configuration of a BU with an area B (variable) from the mother universe with an area A (fixed).

Fig.1 MINBU configuration

The 'neck' of Fig.1 is composed of three links which is the minimum loop in the dynamically triangulated surface. The configuration is called the minimum neck baby universe (MINBU). MINBU distribution for the Liouville-gravity and its matter-coupled case were already measured [5, 6, 13].

First we explain briefly our lattice model of R^2 -gravity. The surface is regularized by the triangulation. The number of vertices ,where some links (edges of triangles) meet, is N_0 . The number of links at the i-th vertex $(i = 1, 2 \cdots, N_0)$ is q_i . The number of triangles (N_2) is related to N_0 as $N_2 = 2N_0 - 4$ for the sphere topology. The discretized model is then described by

$$S_L = -\beta_L \frac{4\pi^2}{3} \sum_{i=0}^{N_0} \frac{(6-q_i)^2}{q_i} = -48\pi^2 \beta_L \sum_i \frac{1}{q_i} + \text{const}$$
 (1)

where β_L is the R²-coupling constant of the lattice model. We do measurement for $\beta_L = 0, 50, 100, 200, 300, -20, -50$. We present the MINBU dstribution of R^2 -gravity with no matter field (pure R²-gravity) in Fig.2 and 3 for $\beta_L \geq 0$ and for $\beta_L \leq 0$ respectively. The total number of triangles is $N_2 = 5000$. For the detail see [11].

Fig.3 MINBU distribution for $\beta_L \leq 0$. Pure R^2 -gravity.

As for positive β_L (Fig.2), we see clearly the transition point P_0 , for each curve, at which the distribution qualitatively changes. For the region $P = B/A > P_0$, the birth probability decreases as the size of BU increases. For the region $P < P_0$, the birth probability increases as the size of BU increases. The value of the transition point P_0 depends on β and increases as β increases. As for negative β (Fig.3), the slope of the curve tends to be sharp as $|\beta|$ increases at least for the region $P < P_1$. The transition point P_1 is not so clear as Fig.2.

In Sect 4.2 we interpret these data theoretically using the semiclassical approach explained in Sect 3.

3 Semiclassical Approach

We analyse the simulation data by the semiclassical approach. The R^2 - gravity interacting with c_m -components scalar matter fields is described by

$$S = \int d^2x \sqrt{g} (\frac{1}{G}R - \beta R^2 - \mu - \frac{1}{2} \sum_{i=1}^{c_m} \partial_a \Phi_i \cdot g^{ab} \cdot \partial_b \Phi_i) \quad , \quad (a, b = 1, 2) \quad , \quad (2)$$

where G is the gravitaional coupling constant, μ is the cosmological constant, β is the coupling strength for R^2 -term and Φ is the c_m - components scalar matter fields. The signature is Euclidean. The partition function, under the fixed area condition $A=\int d^2x\sqrt{g}$ and with the conformal-flat gauge $g_{ab}=e^{\varphi}$ δ_{ab} , is written as [14],

$$\bar{Z}[A] = \int \frac{\mathcal{D}g\mathcal{D}\Phi}{V_{GC}} \{exp_{\bar{h}}^{1}S\} \ \delta(\int d^{2}x\sqrt{g} - A) = exp_{\bar{h}}^{1}(\frac{8\pi(1-h)}{G} - \mu A) \times Z[A] \quad ,$$

$$Z[A] \equiv \int \mathcal{D}\varphi \ e^{+\frac{1}{\bar{h}}S_{0}[\varphi]} \ \delta(\int d^{2}x \ e^{\varphi} - A) \quad ,$$

$$S_{0}[\varphi] = \int d^{2}x \ (\frac{1}{2\gamma}\varphi\partial^{2}\varphi - \beta \ e^{-\varphi}(\partial^{2}\varphi)^{2} + \frac{\xi}{2\gamma}\partial_{a}(\varphi\partial_{a}\varphi) \) \quad , \quad \frac{1}{\gamma} = \frac{1}{48\pi}(26 - c_{m}) \quad (4)$$

where h is the number of handles ¹. V_{GC} is the gauge volume due to the general coordinate invariance. ξ is a free parameter. The total derivative term generally appears when integrating out the anomaly equation $\delta S_{ind}[\varphi]/\delta \varphi = \frac{1}{\gamma} \partial^2 \varphi$. This term

¹ The sign for the action is different from the usual convention as seen in (3).

turns out to be very important. ² We consider the manifold of a fixed topology of the sphere h = 0 and the case $\gamma > 0$ ($c_m < 26$). \hbar is Planck constant. ³

Z[A] is rewritten as, after the Laplace transformation and the inverse Laplace one,

$$Z[A] = \int \frac{d\lambda}{\hbar} \int \mathcal{D}\varphi \, \exp \, \frac{1}{\hbar} [\, S_0[\varphi] - \lambda(\int d^2x e^{\varphi} - A)]$$

$$= \int \frac{d\lambda}{\hbar} e^{\frac{1}{\hbar}\lambda A} \int \mathcal{D}\varphi \, \exp \, \left\{ \frac{1}{\hbar} S_{\lambda}[\varphi] \right\} \quad ,$$

$$S_{\lambda}[\varphi] \equiv S_0[\varphi] - \lambda \int d^2x \, e^{\varphi}$$

$$= \int d^2x \, \left(\frac{1}{2\gamma} \varphi \partial^2 \varphi - \beta \, e^{-\varphi} (\partial^2 \varphi)^2 \, + \frac{\xi}{2\gamma} \partial_a(\varphi \partial_a \varphi) \, - \lambda \, e^{\varphi} \, \right) \quad ,$$

$$(5)$$

where the λ -integral should be carried out along an appropriate contour parallel to the imaginary axis in the complex λ -plane. Note that the δ -function constraint in (3) is substituted by the λ -integral. The leading order configuration is given by the stationary minimum.

$$\frac{\delta S_{\lambda}[\varphi]}{\delta \varphi} \bigg|_{\varphi_{c}} = \frac{1}{\gamma} \partial^{2} \varphi + \beta \{ e^{-\varphi} (\partial^{2} \varphi)^{2} - 2 \partial^{2} (e^{-\varphi} \partial^{2} \varphi) \} - \lambda e^{\varphi} \bigg|_{\varphi_{c}} = 0 ,
\frac{d}{d\lambda} (\lambda A + S_{\lambda}[\varphi_{c}]) \bigg|_{\lambda_{c}} = 0 ,$$

$$Z[A] \approx \frac{1}{\hbar} exp \frac{1}{\hbar} \{ \lambda_{c} A + S_{\lambda_{c}}[\varphi_{c}] \} \equiv \frac{1}{\hbar} exp \frac{1}{\hbar} \Gamma_{c}^{eff} .$$
(6)

Generally this approximation is valid for a large system. In the present case, the system size is proportional to $\frac{4\pi}{\gamma} = \frac{26-c_m}{12}$. We expect the approximation is valid except the region: $c_m \sim 26$.

The solution φ_c and λ_c , which describes the positive-constant curvature solution and is continuous at $\beta = 0$, are given by [7]

$$\varphi_c(r) = -\ln \left\{ \frac{\alpha_c}{8} (1 + \frac{r^2}{A})^2 \right\} , \quad r^2 = (x^1)^2 + (x^2)^2 ,$$

$$\alpha_c = \frac{4\pi}{w} \left\{ w + 1 - \sqrt{w^2 + 1 - 2\xi w} \right\} , \quad w = 16\pi \beta' \gamma , \quad \beta' \equiv \frac{\beta}{A} , \qquad (7)$$

$$\gamma \lambda_c A = \frac{w}{16\pi} (\alpha_c)^2 - \alpha_c ,$$

where ξ must satisfy $-1 \leq \xi \leq +1$ for the realness of α_c . (x^1, x^2) are the flat (plane) coordinates. The partition function at the classical level is given by

$$\Gamma_c^{eff} = \ln Z[A]|_{\hbar^0} = \lambda_c A + (1+\xi) \frac{4\pi}{\gamma} \ln \frac{\alpha_c}{8} - \frac{\alpha_c}{\gamma} w + C(A) ,$$

$$C(A) = \frac{8\pi(2+\xi)}{\gamma} + \frac{8\pi\xi}{\gamma} \{ \ln(L^2/A) - 1 \} + O(A/L^2) ,$$

$$\frac{L^2}{A} \gg 1 ,$$
(8)

where L is the infrared cut-off $(r^2 \leq L^2)$ introduced for the divergent volume integral of the total derivative term. Note that C(A) does not depend on β (or w) but

² The uniqueness of this term, among all possible total derivatives, is shown in [7].

 $^{^3}$ In this section only, we explicitly write \hbar (Planck constant) in order to show the perturbation structure clearly.

on c_m (or γ) and A. Furthermore C(A) has an arbitrary constant of the form $(8\pi\xi/\gamma) \times (\text{const})$ due to the freedom of the choice of the regularization parameter: $L \to (\text{const})' \times L$. This arbitrary constant turns out to be important.

For the case $\beta=0$, the theory is ordinary 2d gravity and we call it Liouville gravity in contrast with R^2 -gravity for $\beta \neq 0$. For the case $c_m=0$, the theory is called the pure gravity in contrast with the matter-coupled gravity $c_m \neq 0$.

4 Semiclassical Analysis of MINBU Distribution

First we explain the free parameter ξ . Recent analysis of the present theory at the (1-loop) quantum level has revealed that it is conformal (the renormalization group beta functions=0) for $w \geq 1$ when we take $\xi = 1$ [8]. Therefore the value $\xi = 1$ has some meaning purely within the theory. The validity of this choice is also confirmed from a different approach, that is, the comparison of the special case β (or w)= 0 (Liouville gravity) of the present result with the corresponding result from the conformal field theory (KPZ result)[9]. The asymptotic behaviour of $Z[A]|_{\hbar^0}$ at w = 0 is given, from (8), as

$$Z[A]|_{\hbar^{0},w=0} = e^{\Gamma_{c}^{eff}}\Big|_{w=0} = exp\{\frac{4\pi}{\gamma}(3-\xi) + (1+\xi)\frac{4\pi}{\gamma}ln\frac{1+\xi}{2} + \frac{8\pi\xi}{\gamma}ln\frac{L^{2}}{A}\} \approx A^{-\frac{8\pi\xi}{\gamma}} \times const = A^{-\frac{26-c_{m}}{6}\xi} \times const ,$$
as $A \to +\infty$. (9)

On the other hand, the KPZ result is

$$Z^{KPZ}[A] \sim A^{\gamma_s - 3}$$
 , $\gamma_s = \frac{1}{12} \{ c_m - 25 - \sqrt{(25 - c_m)(1 - c_m)} \} + 2$. (10)

In order for our result to coincide with the KPZ result in the 'classical limit' $c_m \to -\infty$: $Z^{KPZ}[A] \sim A^{+\frac{1}{6}c_m}$, we must take

$$\xi = 1 \quad , \tag{11}$$

in (9). In the following of this text we take this value. ⁴

The asymptotic behaviour of the present semiclassical result for the Liouville gravity is, taking $\xi = 1$ in (9),

$$Z[A] \sim A^{-\frac{26-c_m}{6}} \times A^{-1} \quad , \quad A \to +\infty \quad ,$$
 (12)

where the additional factor A^{-1} comes from the λ -integral in the expression of Z[A], (5)[12]. Now we compare the KPZ result and the semiclassical result in the normalized form.

$$Z_{norm}^{KPZ}[A] \equiv \frac{Z^{KPZ}[A]}{Z^{KPZ}[A]|_{c_m=0}} \sim A^{\gamma_s(c_m)-\gamma_s(c_m=0)} ,$$

$$\gamma_s(c_m) - \gamma_s(c_m=0) = \frac{1}{12} \{c_m + 5 - \sqrt{(25 - c_m)(1 - c_m)}\} ,$$

$$Z_{norm}[A] \equiv \frac{Z[A]}{Z[A]|_{c_m=0}} \sim A^{+\frac{c_m}{6}} .$$
(13)

⁴ In the numerical evaluation, we take $\xi = 0.99$ for the practical reason.

We can numerically confirm that the semiclassical result, $\frac{c_m}{6}$, and the KPZ result, $\gamma_s(c_m) - \gamma_s(c_m = 0)$, have very similar behaviour for the region $c_m \leq 1[12]$.

Now we go back to the general value of β . The birth-probability of the baby universe with area B(0 < B < A/2) from the mother universe with the total area A is given by [4]

$$n_{A}(B) = \frac{3(A - B + a^{2})(B + a^{2})Z[B + a^{2}]Z[A - B + a^{2}]}{A^{2} \times Z[A]}$$

$$\approx \frac{3(1 - p)pZ[pA]Z[(1 - p)A]}{Z[A]} , \qquad (14)$$

$$\ln \left(\frac{n_{A}(B)}{3}\right) \approx \ln (1 - p)p + \ln Z[pA] + \ln Z[(1 - p)A] - \ln Z[A] ,$$

$$p \equiv \frac{B}{A} , \quad 0$$

We apply the result of Z[A] in Sect.3 to the above expressions.

4.1 c_m -dependence

First we present the semiclassical prediction for Liouville gravity ($\beta = 0$). The result (8) for the case $\beta = 0$ gives ,taking $\xi = 1$,

$$\gamma \ln Z[rA] = 8\pi (\ln \pi + 1) + 8\pi \ln(\frac{1}{r} \cdot \frac{L^2}{A})$$
 (15)

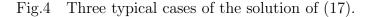
Then the MINBU distribution normalized by the pure garvity $(c_m = 0)$ is obtained as

$$\frac{n_A(B)}{n_A(B)|_{c_m=0}} = \{p(1-p)\}^{\frac{c_m}{6}} \times \exp\{\frac{c_m}{12} \times \Delta\} ,
\Delta \equiv -2(\ln \pi + 1) - 2\ln\frac{L^2}{A} ,$$
(16)

where Δ can be regarded as the free real parameter due to the arbitrariness of the infrared regularization parameter L. We know from the result (16) that the MINBU distribution lines for different c_m 's cross at the single point $p = p^*$ given by

$$p^*(1-p^*) = \exp\{-\frac{1}{2}\Delta\}$$
 , $p^* < \frac{1}{2}$. (17)

Fig.4 shows three typical cases of p^* .



The choice of Δ is important to fit the theoretical curve (16) with the data. We show the behaviour of (16) for the three cases: 1) $\exp(-\frac{1}{2}\Delta) \ll \frac{1}{4}$, Near Point O,Fig.5a; 2) $\exp(-\frac{1}{2}\Delta) > \frac{1}{4}$, Above Point A, Fig.5b; 3) $\exp(-\frac{1}{2}\Delta) = \frac{1}{4} - 0$, Near Point A, Fig.5c.

Fig.5a MINBU distribution for Liouville gravity, $\Delta = 8$

Fig.5b MINBU distribution for Liouville gravity, $\Delta=1$

Fig.5c MINBU distribution for Liouville gravity, $\Delta = 3$

Fig.5a well fits with the known result of the computer simulation[5, 13]. This result shows the importance of the infrared regularization.

4.2 β -dependence

We consider the pure gravity $(c_m = 0)$. We plot MINBU dstribution, $\ln n_A(B)$, as the function of p ($0.001) for various cases of <math>\beta' = \beta/A$ ($\xi = 0.99$). Fig.6a and 6b show that for $\beta' > 0$ and $\beta' < 0$ respectively.

Fig.6a MINBU distribution for $\beta' \geq 0$. $\xi = 0.99, c_m = 0$.

Fig.6b MINBU distribution for
$$\beta' \leq 0$$
. $\xi = 0.99, c_m = 0$.

The above results of Fig.6a and Fig.6b qualitatively coincide with those of Fig.2 and Fig.3, respectively.

We list the asymptotic behaviour of $\ln n_A(B)$ for the general ξ and c_m in Table 1.

Phase	(C) 0	(B) $ w \ll p$	(A) 0
$\alpha_p^-(pA)$	$8\pi\{1+\frac{1-\xi}{2}\frac{p}{w}\}$	$4\pi(1+\xi)\{1-\frac{1-\xi}{2}\frac{w}{p}\}$	$\frac{4\pi(1+\xi)p}{w}$ \times
	$+O(\frac{p^2}{w^2})$	$+O(\frac{w^2}{p^2})$	$\{1+O(\frac{p}{w})\}$
	$(1-\frac{8\pi\xi}{\gamma})\ln p$	$(1-\frac{8\pi\xi}{\gamma})\ln p$	$\{1 - \frac{4\pi(1-\xi)}{\gamma}\} \ln p$
$\ln n_A(B)$	$-\frac{4\pi}{\gamma}\frac{w}{p}$	$+O(\frac{w}{p})$	$-\frac{4\pi(1+\xi)}{\gamma} \ln w$
	$+O(\frac{p}{w})$	+SmallTerm	$+O(\frac{p}{w})$
	+SmallTerm		+SmallTerm

Table 1 Asymp. behaviour of MINBU distribution, (14), for general
$$c_m$$
 and ξ . $R > 0$, $w \equiv 16\pi\beta'\gamma$, $\gamma = \frac{48\pi}{26-c_m} > 0$, $p = \frac{B}{A}$, $0 , $|w| \lesssim 1$, SmallTerm = const + $O(wp)$ + $O(p)$.$

We characterize each phase in Table 1 as follows.

(A) 0 : Smoothly Creased Surface ⁵

The smoothing term, R^2 , dominates the main configuration and the surface is smooth. The left part $P < P_0(w)$ for each curve (w) in Fig.6a corresponds to this phase. The small BU is harder to be born because it needs high-curvature locally. The large BU is energetically preferable to be born. The area constraint is not effective in this phase. The characteristic scale is β .

(B) $|w| \ll p$: Fractal Surface

The randomness dominates the configuration. The size of BU is so enough large that the R^2 -term is not effective. The area constraint is neither effective. There is no characteristic scale. The right part $P > P_0(w)$ for each curve (w) in Fig.6a and the right part $P > P_1(w)$ for each curve (w) in Fig.6b correspond to this phase. The MINBU distribution is mainly determined by the random distribution of the surface configuration[15].

(C) 0 : Rough Surface ⁶

Due to the large negative value of R^2 -coupling, the configuration with the large curvature is energetically preferable on the one hand, it is strongly influenced by the area constraint on the other hand. Therefore the large BU is much harder to be born than (B) because it has a small curvature and a large area. The small BU

⁵ In [7] we called it Free Creased Surface because this is the phase where the free kinetic term $(R^2$ -term) dominates.

⁶ In [7] we called it Strongly Tensed Perfect Sphere because the surface tension is negatively large and the shape of the whole surface is near a sphere. At the same time the surface tend to become sharp-pointed because it increases the curvature. We call the surface under this circumstace, simply, Rough Surface.

is much easier to be born than (B) because it has a large curvature and a small area. The left part $P < P_1(w)$ for each curve (w) in Fig.6b corresponds to this phase. The characteristic scale is the total area A.

We see the phase structure of Table 1 is the same as that of [7] by the substitution of w by w/p. Although both simulations measure the same surface property, the cross-over phenomenon,however, appears differently. In [7] the physical quantity $<\int d^2x \sqrt{g}R^2>$ is taken to see the surface property. The cross-over can be seen only by measuring for a range of w and the transition point is given by a certain value $|w^*|\approx 1$. This is contrasting with the present case. The cross-over can be seen for any w. The transition is seen at the point p^* , in the MINBU distribution, given by $|w|/p^*\approx 1$. We understand as follows. The MINBU distribution measures the surface at many different 'scales' B, whereas the quantity $<\int d^2x \sqrt{g}R^2>$ measures the surface at a fixed 'scale' (B_1 (or p_1) in the MINBU terminology).

4.3 General Case

We consider the general case of c_m and β . This general case is not yet measured by the Monte Carlo simulation. We present the semiclassical prediction. The analysis so far shows the normalization ((13) and (16)) and the choice of an arbitrary constant due to the infrared regularization (16) are important for the quantitative adjustment. Here, however, we are content with the qualitative behaviour. We do not do the normalization and we ignore the $\ln \frac{L^2}{A}$ term in the evaluation of this subsection.

(1) c_m -dependence We stereographically show MINBU distributions for the range: $0.001 \le p \le 0.2, \ -24 \le c_m \le +24$, in Fig.7a($\beta'=0$), Fig.7b($\beta'=+10^{-4}$) and Fig.7c($\beta'=-10^{-5}$).

Fig.7a MINBU distribution for
$$0.001 \le p \le 0.2, -30 \le c_m \le +24$$
.
 $\beta' = 0, \xi = 0.99$.

Fig.7b MINBU dstribution for
$$0.001 \le p \le 0.2, -30 \le c_m \le +24$$
.
 $\beta' = +10^{-4}, \xi = 0.99$.

Fig.7c MINBU dstribution for
$$0.001 \le p \le 0.2, -30 \le c_m \le +24$$
.
 $\beta' = -10^{-5}, \xi = 0.99$.

No 'ridge' appears in Fig.7a. From this, we see matter fields affect the surface dynamics homogeneously at all scales. (This result is natural because the matter coupling constand c_m does not have the scale dimension.) The slope along the p-axis continuously decreases as c_m increases. In Fig.7b, a ridge runs from a low p to a high p as c_m increases. In Fig.7c,a 'hollow' runs from a high p to a low p as c_m increases. The ridge and the hollow correspond to the series of the cross-over points. In both Fig.7b and Fig.7c, the cross-over becomes dimmer as c_m increases and becomes sharper as c_m decreases.

(2) β -dependence

We stereographically show MINBU distributions for the range: $0.001 \le p \le 0.2, -10^{-5} \le \beta' \le +10^{-4}$, in Fig.8a($c_m = 0$), Fig.8b($c_m = +10$) and

Fig.8c(
$$c_m = -10$$
).

Fig.8a MINBU distribution for
$$0.001 \le p \le 0.2$$
, $-10^{-5} \le \beta' \le +10^{-4}$. $c_m = 0, \xi = 0.99$.

Fig.8b MINBU dstribution for
$$0.001 \le p \le 0.2, -10^{-5} \le \beta' \le +10^{-4}$$
. $c_m = +10, \xi = 0.99$.

Fig.8c MINBU dstribution for
$$0.001 \le p \le 0.2, -10^{-5} \le \beta' \le +10^{-4}$$
. $c_m = -10, \xi = 0.99$.

The Fig.8a corresponds to the stereographic display of Fig.6a and 6b. In each of Fig.8a-c, a ridge appears for $\beta'>0$. For $\beta'<0$, a tower appears instead of a ridge. For a large positive c_m (matter dominated region, $c_m=10$ in Fig.8b) the undulation of the MINBU dstribution surface ⁷ is small(the cross-over is dim), whereas it is large(the cross-over is sharp) for a large negative c_m (matter anti-dominated region, $c_m=-10$ in Fig.8c).

⁷Do not confuse it with the 2d manifold which the present model of gravity represents.

5 Discussion and Conclusion

In the (2d) QG, at present, there exists no simple way to find good physical observables. They have been found by 'try and error'. MINBU is one of good observables to measure the surface property. Quite recently a new observable ,the 'electric resistivity' of the surface, is proposed by [16]. By measuring the observable for the matter-coupled Liouville gravity, they observe a cross-over ,near $c_m = 1$, from the surface where a complex-structure is well-defined to the surface where it is not well-defined. The analysis of the new obserbable, from the standpoint of the present approach, is important.

There are some straightforward but important applications of the present analysis: 1) higher-genus case, 2) the case with other higher-derivative terms such as R^3 and $\nabla R \cdot \nabla R$, 3) the quantum effect. As for 2) ,references [17] and [18] have already obtained the Monte Carlo data.

We have presented the numerical result of MINBU and its theoretical explanation using the semiclassical approximation. The surface properties are characterized. It is confirmed that the present lowest approximation is very efficient to analyse 2d quantum gravity, at least, qualitatively.

Finally we expect other new observables will be found and many Monte Carlo measurements will be done ,including 3 and 4 dimensional cases, next a few years. The interplay between the measurement by the computer simulation and the theoretical interpretation will become important more and more. We believe this process will lead to the right understanding of the (Euclidean) quantum gravity.

Acknowledgement

The authors thank N. Ishibashi and H. Kawai for comments and discussions about the present work.

References

- [1] J.Ambjørn,B.Durhuus and J.Fröhlich,Nucl.Phys.**B257**[FS13] (1985)433
- $[2] \ F. David, Nucl. Phys. \textbf{B257} [FS14] (1985) 543$
- [3] V.A.Kazakov, I.K.Kostov and A.A.Migdal, Phys.Lett. B157 (1985)295
- [4] S.Jain and S.D.Mathur, Phys.Lett. B286 (1992) 239
- [5] J.Ambjørn, S.Jain and G.Thorleifsson, Phys.Lett. ${\bf B307} (1993)34$
- [6] G.Thorleifsson, "Baby universe and fractal structure of 2 d gravity", NBI-HE-93-68
- [7] S.Ichinose,N.Tsuda and T.Yukawa,Preprint of Univ.of Shizuoka, US-94-03,hep-th/9502101,to be published in Nucl.Phys.B,"Classical Solution of Two Dimensional R^2 -Gravity and Cross-Over Phenomenon"
- [8] S.Ichinose, Preprint of SLAC, SLAC-PUB-95-6774, to be published in Nucl. Phys.B, "Renormalization of Two Dimensional \mathbb{R}^2 -Gravity"

- [9] V.G.Knizhnik, A.M.Polyakov and A.B.Zamolodchikov, Mod. Phys. Lett. A3(1988)819
- [10] D.V.Boulatov and V.A.Kazakov, Phys.Lett.**B184**(1987)247
- [11] N.Tsuda and T.Yukawa, Phys. Lett. **B305**(1993)223
- [12] S.Ichinose, Preprint of Univ. of Shizuoka, US-95-06, "Thermodynamic Properties, Phases and Classical Vacua of Two Dimensional \mathbb{R}^2 -Gravity"
- [13] J.Ambjørn and G.Thorleifsson, Phys. Lett. **B323**(1994)7
- [14] A.M.Polyakov, Phys. Lett. **103B**(1981) 207
- [15] E.Brézin, C.Itzykson, G.Parisi and J.B.Zuber, Commun. Math. Phys. 59 (1978) 35
- [16] H.Kawai, N.Tsuda and T.Yukawa, "Complex Structures defined on Dynamically Triangulated Surfaces", KEK-TH-429, TIT/HEP-286
- [17] N.Tsuda and T.Yukawa, private communication
- [18] N.Tsuda, Doctor thesis, Tokyo Institute of Technology, 1994

Figure Captions

- Fig.1 MINBU configuration.
- Fig.2 MINBU distribution for $\beta_L \geq 0$, Pure R^2 -gravity.
- Fig.3 MINBU distribution for $\beta_L \leq 0$. Pure R^2 -gravity.
- Fig.4 Three typical cases of the solution of (17).
- Fig.5a MINBU distribution for Liouville gravity, $\Delta = 8$.
- Fig.5b MINBU distribution for Liouville gravity, $\Delta = 1$.
- Fig.5c MINBU distribution for Liouville gravity, $\Delta = 3$.
- Fig.6a MINBU distribution for $\beta' \geq 0$. $\xi = 0.99, c_m = 0$.
- Fig.6b MINBU distribution for $\beta' \leq 0$. $\xi = 0.99, c_m = 0$.
- Fig.7a MINBU distribution for $0.001 \le p \le 0.2, -30 \le c_m \le +24$. $\beta' = 0, \xi = 0.99$.
- Fig.7b MINBU dstribution for $0.001 \le p \le 0.2, -30 \le c_m \le +24$. $\beta' = +10^{-4}, \xi = 0.99$.
- Fig.7c MINBU distribution for $0.001 \le p \le 0.2, -30 \le c_m \le +24$. $\beta' = -10^{-5}, \xi = 0.99$.
- Fig.8a MINBU distribution for $0.001 \le p \le 0.2, -10^{-5} \le \beta' \le +10^{-4}$. $c_m = 0, \xi = 0.99$.
- Fig.8b MINBU dstribution for $0.001 \le p \le 0.2, -10^{-5} \le \beta' \le +10^{-4}$. $c_m = +10, \xi = 0.99$.
- Fig.8c MINBU dstribution for $0.001 \le p \le 0.2, -10^{-5} \le \beta' \le +10^{-4}$. $c_m = -10, \xi = 0.99$.

This figure "fig1-1.png" is available in "png" format from:

This figure "fig2-1.png" is available in "png" format from:

This figure "fig1-2.png" is available in "png" format from:

This figure "fig2-2.png" is available in "png" format from:

This figure "fig1-3.png" is available in "png" format from:

This figure "fig2-3.png" is available in "png" format from: